

ChemComm

Accepted Manuscript



This is an *Accepted Manuscript*, which has been through the Royal Society of Chemistry peer review process and has been accepted for publication.

Accepted Manuscripts are published online shortly after acceptance, before technical editing, formatting and proof reading. Using this free service, authors can make their results available to the community, in citable form, before we publish the edited article. We will replace this *Accepted Manuscript* with the edited and formatted *Advance Article* as soon as it is available.

You can find more information about *Accepted Manuscripts* in the [Information for Authors](#).

Please note that technical editing may introduce minor changes to the text and/or graphics, which may alter content. The journal's standard [Terms & Conditions](#) and the [Ethical guidelines](#) still apply. In no event shall the Royal Society of Chemistry be held responsible for any errors or omissions in this *Accepted Manuscript* or any consequences arising from the use of any information it contains.



ChemComm

COMMUNICATION

Hierarchical porous anatase TiO₂ derived from a titanium metal-organic framework as superior anode materials for lithium ion batteries

Received 00th January 20xx,
Accepted 00th January 20xx

DOI: 10.1039/x0xx00000x

www.rsc.org/

Zhiliang Xiu^{a,b}, Muhammad Hilmy Alfaruqi^a, Jihyeon Gim^a, Jinju Song^a, Sungjin Kim^a, Trang Vu Thi^a, Pham Tung Duong^a, Joseph Paul Baboo^a, Vinod Mathew^a, Jaekook Kim^{*a}

Hierarchical meso-/macroporous anatase TiO₂ was synthesized from the hydrolysis of a titanium metal-organic framework precursor followed by calcination in air. This unique porous feature enables the superior rate capability and excellent cycling stability of anatase TiO₂ as an anode for rechargeable lithium-ion batteries.

Rechargeable lithium-ion batteries (LIBs) have been widely applied in portable electronics, electric vehicles, and stationary energy storage systems.¹⁻³ Titanium dioxide (TiO₂) is a particularly attractive electrode material for large scale energy storage because it is an abundant resource, low cost, and environmentally friendly.⁴ Moreover, anatase TiO₂ exhibits a higher lithium insertion-extraction potential of ~1.6 V vs. Li/Li⁺ to ensure that it is safe enough. It achieves this safety by avoiding the formation of solid electrolyte interface (SEI) layers and lithium plating on the negative electrode compared with the conventional graphite anode materials. It is also structurally stable as its volume only changes slightly (< 4%) during the lithium ion insertion/extraction process. This stability results in long cycle time and durability. However, the inherent poor electronic conductivity and sluggish lithium ion diffusion limits its practical application for high power outputs.⁵

An effective way to enhance the high rate performance of the electrode is to prepare porous structures which facilitate the fast transport of lithium ions and electrons.⁶ Microporous electrode materials with diameters of less than 2 nm possess high surface area. However, the small pores may be easily blocked and the

electrolyte ions may not fully penetrate into the electrode structure.⁷ While mesopores electrode with diameters in the range of 2-50 nm offers a high surface area, good pore accessibility and large amount of electroactive sites.⁸ Macropores with diameters of more than 50 nm can effectively accommodate electrolytes for an electrochemical reaction.⁹ Thus, generating a hierarchical porous structure with mesopores and macropores is a promising strategy to improve the rate performance of the electrode.

Metal-organic frameworks (MOFs) are a new class of inorganic-organic hybrid functional materials with high porosity, a large surface area and tunable pore structure.¹⁰⁻¹² In recent years, MOFs have been widely applied as templates/precursors to prepare hollow/porous metal oxides by thermal decomposition. When utilized as anode materials for LIBs, these MOFs-derived hollow/porous metal oxides exhibited superior electrochemical performance for lithium storage.¹³⁻¹⁵ For instance, the porous anatase TiO₂ was prepared through the calcination of a titanium metal-organic framework precursor (MIL-125 (Ti)) in an air atmosphere and exhibited high capacity retention and good rate capability.¹⁶ Rutile TiO₂ embedded in carbon submicron-tablets with a "blueberry muffin" morphology was fabricated *via* a two-step pyrolysis from the MIL-125 (Ti) and showed high reversible capacity, superior rate capability and excellent long-term cycling stability.¹⁷ However, the obtained metal oxides mostly possessed small pores (micropores or mesopores) and narrow pore size distribution, which failed to attain full lithium storage capability.

In this paper, we propose a new mild method to prepare hierarchical porous anatase TiO₂ (HPT) from the hydrolysis of MIL-125 (Ti) followed by calcination in air atmosphere. The HPT possesses bimodal pores of mesopores and macropores. By combining the merits bimodal characteristics, the HPT is expected to significantly improve the battery performance.

The synthetic process of HPT involves three steps. The experimental details are listed in the ESI. Firstly, MIL-125 (Ti) was synthesized by a solvothermal method according to the previous literature.¹⁸ X-ray diffraction (XRD) pattern of the as-synthesized MIL-125 (Ti) (Fig. S1b, ESI) well complies with the simulated MIL-

^aDepartment of Materials Science and Engineering, Chonnam National University, 300 Yongbong dong, Buk-gu, Gwangju 500-757, South Korea. Email: jaekook@chonnam.ac.kr

^bShandong Provincial Key Laboratory of Processing and Testing Technology of Glass & Functional Ceramics, Key Laboratory of Amorphous and Polycrystalline Materials, Qilu University of Technology, Jinan 250353, P.R. China. Electronic Supplementary Information (ESI) available: Experimental details; XRD patterns of simulated MIL-125 (Ti), as-synthesized MIL-125 (Ti), as-refluxed TiO₂, and HPT; FT-IR spectra of as-synthesized MIL-125 (Ti), as-refluxed TiO₂, and HPT; SEM images of MIL-125 (Ti) and as-refluxed TiO₂; TGA curve of HPT; N₂ adsorption-desorption isotherm and corresponding pore size distribution of MT. See DOI: 10.1039/x0xx00000x

125 (Ti) (Fig. S1a, ESI). The sharp and strong peaks indicate that the as-synthesized MIL-125 (Ti) is well crystallized. Fourier transform infrared (FT-IR) spectrum (Fig. S2a, ESI) reveals that there exist typical vibrational bands of carboxylic acid functional groups in the range of 1300-1800 cm^{-1} , benzene rings in the range of 700-1200 cm^{-1} and O-Ti-O in the range of 400-800 cm^{-1} .¹⁹ Scanning electron microscope (SEM) images (Fig. S3, ESI) illustrate that the MIL-125 (Ti) crystal comprises nanosized particles with truncated octahedron morphologies. The MIL-125 (Ti) powders seem to be light and fluffy, indicating low bulky density. Then the as-synthesized MIL-125 (Ti) was refluxed in water. The as-refluxed sample is a typical anatase TiO_2 phase (JCPDS, No. 21-1272) with relatively low crystallinity as can be seen from the XRD pattern (Fig. S1c, ESI). The FT-IR spectrum (Fig. S2b, ESI) indicates that few residual organic linkers still remain in the as-refluxed sample. SEM images (Fig. S4, ESI) show that the precursor is broken down into irregular aggregates consisted of nanoparticles. Finally, the as-refluxed TiO_2 was calcined at 400 °C in air to remove the residual organic linkers. In addition, the calcined sample reveals an enhancement in particle crystallinity while retains the pure anatase TiO_2 phase, as observed from the corresponding XRD pattern (Fig. S1d, ESI). Moreover, the disappearance of the typical vibrational bands corresponding to the organic linkers in the FT-IR spectrum of the calcined sample (Fig. S2c, ESI) indicates that the MIL-125 (Ti) is transformed to the pure anatase-type TiO_2 . However, the emergence of intensive and weak bands at 3000-3600 cm^{-1} and 1600-1700 cm^{-1} corresponding to the stretching and deformation vibration (H-O-H), respectively, of hydroxyl groups appear to suggest that water molecules may be easily adsorbed inside the HPT structure due to the high particle surface area.²⁰ Moreover, the thermogravimetric analysis (TGA) curve (Fig. S5) reveals the presence of a small amount (~ 1.4 wt%) of adsorbed water molecules in the calcined sample.

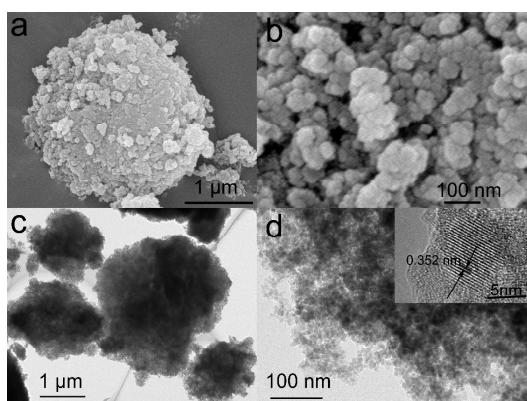


Fig. 1 SEM images of (a, b) and TEM images of HPT. Inset in (d) is the HRTEM image of HPT.

SEM image of HPT (Fig. 1a) reveals that the final products are bulk aggregates with no regular morphology. There are lots of pores on the surface of HPT and these are visible in the high-magnification SEM image (Fig. 1b). Transmission electron microscopy (TEM) images in Fig. 1c and d further confirm the typical hierarchical pore

structure for the HPT sample assembled with ultrafine particles of several nanometers in size. The high-resolution transmission electron microscopy (HRTEM) image (inset in Fig. 1d) clearly reveals the lattice fringes of 0.352 nm which corresponds well with the interplanar spacing of the anatase TiO_2 (101) plane.

Fig. 2 shows the N_2 adsorption-desorption isotherm and Barrett-Joyner-Halenda (BJH) pore size distribution of HPT. A distinct hysteresis in the larger range of ca. 0.7–1.0 P/P_0 indicates the presence of mesopores and macropores.²¹ The pore size distribution shows bimodal and hierarchical porosity: mesopores with pore diameters of 12, 16 and 28 nm along with macropores with pore diameters of up to 185 nm. The Brunauer-Emmett-Teller (BET) surface area and total pore volume of the HPT are 147 $\text{m}^2 \text{g}^{-1}$ and 0.6238 $\text{cm}^3 \text{g}^{-1}$, respectively. The TiO_2 prepared through the direct calcination of MIL-125 (Ti) in air shows the characteristic of mesoporous material with average pore diameters of 4 nm (Fig. S6, ESI). Its surface area and total pore volume are 124 $\text{m}^2 \text{g}^{-1}$ and 0.1771 $\text{cm}^3 \text{g}^{-1}$, respectively. The HPT exhibits a much higher surface area and pore volume compared to the mesoporous TiO_2 (MT).

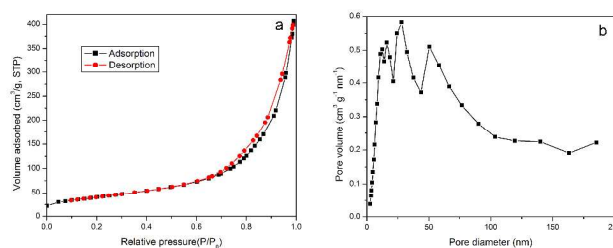
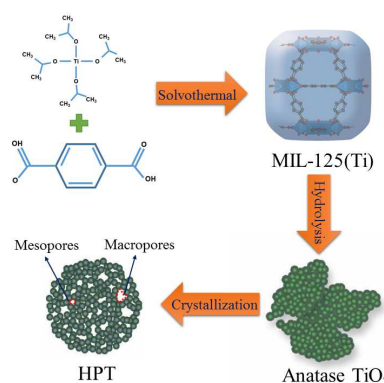


Fig. 2 N_2 adsorption-desorption isotherm of HPT (a) and corresponding pore size distribution (b).



Scheme 1 Schematic illustration of the formation mechanism of HPT

The formation mechanism of HPT is illustrated in Scheme 1. MIL-125 (Ti) is built up with eight TiO_6 octahedron units connected by terephthalate linkers forming a three-dimensional microporous networks. The coordination bond strength between them is relatively weak.²² Once the MIL-125 (Ti) is refluxed in the water, water can readily penetrate the microporous channel and promptly

react with MIL-125 (Ti) to form TiO_2 nuclei for further growth.²³ The density difference between MIL-125 (Ti) and TiO_2 can readily generate cracks in the MIL-125 (Ti) crystal, which will break the precursor into pieces with irregular morphology. The broken pieces further agglomerate into bulk aggregates. Anatase TiO_2 has higher lattice density than MIL-125 (Ti), so the micropores in the MIL-125 (Ti) will be enlarged to be smaller mesoporous within each broken pieces. Larger mesopores and macropores may be generated from the interaggregation of the broken pieces. Finally, the as-refluxed TiO_2 was calcined in air to get the highly crystallized HPT.

Electrochemical performance of HPT was investigated as an anode material for LIBs within a voltage range of 1.0–3.0 V vs. Li^+/Li . The cyclic voltammogram (CV) of the HPT anode at a scan rate of 0.1 mV s^{-1} from 1.0–3.0 V is shown in Fig. 3a. A pair of cathodic/anodic peaks at 1.62 and 2.12 V correspond to a lithium insertion/extraction reaction in anatase.²⁴ Fig. 3b displays the discharge-charge voltage profiles of the HPT electrode for the first five cycles at a current rate of 0.1 C ($1 \text{ C} = 168 \text{ mA g}^{-1}$). Two distinct plateaus can be clearly observed at 1.75 and 1.90 V correspond to the discharging (Li insertion) and charging (Li extraction) process, respectively. Each discharge profile can be divided into three stages. The first stage is marked by a fast drop in voltage from the open-circuit potential to 1.75 V, which corresponds to a solid solution insertion mechanism related to the small nanocrystallite size and porous nanostructures.²⁵ The second stage is a horizontal plateau region at $\sim 1.75 \text{ V}$, that indicates two phase electrochemical reactions.²⁶ The final stage is a slope-like region linked to the Li^+ storage at the surface as well as the formation of the LiTiO_2 phase.²⁷ The initial discharge and charge capacities of the HPT electrode are 304 and 219 mA h g^{-1} , respectively. The irreversible capacity loss of $\sim 28\%$ is mainly caused by the insertion of some Li^+ into sites that are not extractable and due to the decomposition of trace water adsorbed on the TiO_2 electrode surfaces.²⁸ After five cycles, Coulombic efficiency increases to 95.8%, indicating good reversibility of the electrochemical reactions. The rate performance of the HPT electrode, the MT electrode and the nanosized TiO_2 (NT) electrode at different current rates from 0.1 C to 10 C are shown in Fig. 3c. It is obvious that the HPT sample exhibits superior rate capability compared to the MT sample and the NT sample at each rate. For instance, at a rate of 5 C, the specific discharge capacity of the HPT electrode is about 155 mA h g^{-1} , which is more than the capacity of the MT (120 mA h g^{-1}) and the NT (20 mA h g^{-1}) electrode. Although the HPT sample has a smaller surface area ($147 \text{ m}^2 \text{ g}^{-1}$) compared to the porous anatase TiO_2 ($220 \text{ m}^2 \text{ g}^{-1}$) constructed from MIL-125 (Ti) reported by Chen's group,¹⁶ it exhibits better rate capability. The high rate capability of the HPT electrode can be attributed to the special hierarchical porous nanoarchitecture, which provides shorter transport lengths for both electronic and Li^+ transport as well as the higher electrode-electrolyte contact area. More importantly, after the high rate measurements, the specific capacity of the HPT electrode at 0.1 C can recover to the initial value, demonstrating the excellent structural stability of the sample. The cycling behavior of the HPT electrode at a current rate of 5 C is shown in Fig. 3d. As expected, the HPT electrode exhibits superior capacity retention with $\sim 6.5\%$ capacity loss and high Coulombic efficiency over 99.7% after 200 cycles, which benefits from the high stability of the hierarchical

porous nanoarchitecture and the good accommodation of volume/strain changes during the lithium insertion-extraction process.

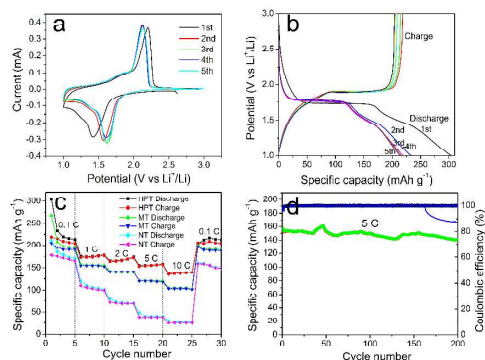


Fig. 3 (a) Cyclic voltammograms of HPT at a scan speed of 0.1 mV s^{-1} . (b) Discharge/charge voltage profiles of HPT at a rate of 0.1 C ($1 \text{ C} = 168 \text{ mA g}^{-1}$). (c) Rate dependent cycling performances of HPT, MT and NT. (d) Cycle performance of HPT at 5 C with a Coulombic efficiency.

In summary, a simple and mild method was applied to prepare anatase TiO_2 with hierarchical bimodal meso-/macroporous structure via the hydrolysis of MIL-125 (Ti) followed by calcination in air. The HPT exhibited superior rate capability compared to the MT and the NT counterparts. Moreover, the HPT presented excellent long-term cycling stability. After 200 cycles at 5 C charging/discharging rates, the capacity loss was only $\sim 6.5\%$. The superior rate capability and excellent cycling stability make HPT a promising anode material for fast rechargeable LIBs.

This work was supported by the National Research Foundation of Korea (NRF) grant funded by the Korea government (MSIP) (2014R1A2A1A10050821).

Notes and references

- H. Li, Z. Wang, L. Chen and X. Huang, *Adv. Mater.*, 2009, **21**, 4593–4607.
- M. Endo, C. Kim, K. Nishimura, T. Fujino and K. Miyashita, *Carbon*, 2000, **38**, 183–197.
- V. Etacheri, R. Marom, R. Elazari, G. Salitra and D. Aurbach, *Energy Environ. Sci.*, 2011, **4**, 3243–3262.
- G.-N. Zhu, Y.-G. Wang and Y.-Y. Xia, *Energy Environ. Sci.*, 2012, **5**, 6652.
- J.-Y. Shin, J. H. Joo, D. Samuelis and J. Maier, *Chem. Mater.*, 2011, **24**, 543–551.
- W. Zhu, H. Yang, K. Nakanishi, K. Kanamori and X. Guo, *RSC Adv.*, 2015, **5**, 24803–24813.
- C. M. Doherty, R. A. Caruso, B. M. Smarsly, P. Adelhelm and C. J. Drummond, *Chem. Mater.*, 2009, **21**, 5300–5306.
- H.-E. Wang, H. Cheng, C. Liu, X. Chen, Q. Jiang, Z. Lu, Y. Y. Li, C. Y. Chung, W. Zhang, J. A. Zapien, L. Martinu and I. Bello, *J. Power Sources*, 2011, **196**, 6394–6399.
- J. S. Sakamoto and B. Dunn, *J. Mater. Chem.*, 2002, **12**, 2859–2861.
- Y. Fu, D. Sun, Y. Chen, R. Huang, Z. Ding, X. Fu and Z. Li, *Angew. Chem. Int. Ed.*, 2012, **51**, 3364–3367.

COMMUNICATION

Journal Name

- 11 Z. Zhang, Y. Chen, X. Xu, J. Zhang, G. Xiang, W. He and X. Wang, *Angew. Chem. Int. Ed.*, 2014, **53**, 429-433.
- 12 Y. Liu, V. C. Kravtsov, R. Larsen and M. Eddaoudi, *Chem. Commun.*, 2006, **14**, 1488-1490.
- 13 J. Sun, Q. Xu, *Energy Environ. Sci.*, 2014, **7**, 2071-2100.
- 14 L. Lux, K. Williams and S. Ma, *Cryst. Eng. Comm*, 2015, **17**, 10-22.
- 15 W. Xia, A. Mahmood, R. Zou and Q. Xu, *Energy Environ. Sci.*, 2015, DOI: 10.1039/C5EE00762C.
- 16 Z. Wang, X. Li, H. Xu, Y. Yang, Y. Cui, H. Pan, Z. Wang, B. Chen and G. Qian, *J. Mater. Chem. A*, 2014, **2**, 12571.
- 17 P. Wang, J. Lang, D. Liu and X. Yan, *Chem. Commun.*, 2015, DOI: 10.1039/c0xx00000x.
- 18 M. Dan-Hardi, C. Serre, T. Frot, L. Rozes, G. Maurin, C. Sanchez and G. Férey, *J. Am. Chem. Soc.*, 2009, **131**, 10857-10859.
- 19 S. Hu, M. Liu, K. Li, Y. Zuo, A. Zhang, C. Song, G. Zhang, X. Guo, *Cryst. Eng. Comm.*, 2014, **16**, 9645-9650.
- 20 T. Bezrodnaa, G. Puchkovskaa, V. Shymanovskaa, J. Baranb, H. Ratajczak, *J. Mol. Struct.*, 2004, **700**, 175-181.
- 21 C. Gao, G. Chen, X. Wang, J. Li, Y. Zhou and J. Wang, *Chem. Commun.*, 2015, **51**, 4969-4972.
- 22 C. W. Abney, K. M. L. Taylor-Pashow, S. R. Russell, Y. Chen, R. Samantaray, J. V. Lockard and W. Lin, *Chem. Mater.*, 2014, **26**, 5231-5243.
- 23 L. Zhong, J. Hu, L. Wan, W. Song, *Chem. Commun.*, 2008, **10**, 1184-1186.
- 24 H. Lindström, S. Södergren, A. Solbrand, H. Rensmo, J. Hjelm, A. Hagfeldt and S.-E. Lindquist, *J. Phys. Chem. B*, 1997, **101**, 7717-7722.
- 25 G. Sudant, E. Baudrin, D. Larcher and J.-M. Tarascon, *J. Mater. Chem.*, 2005, **15**, 1263-1269.
- 26 U. Lafont, D. Carta, G. Mountjoy, A. V. Chadwick and E. M. Kelder, *J. Phys. Chem. C*, 2010, **114**, 1372-1378.
- 27 M. Wagemaker, W. J. H. Borghols and F. M. Mulder, *J. Am. Chem. Soc.*, 2007, **129**, 4323-4327.
- 28 H. E. Wang, Z. G. Lu, L. J. Xi, R. G. Ma, C. D. Wang, J. A. Zapien and I. Bello, *ACS Appl. Mater. Inter.*, 2012, **4**, 1608-1613.